

promoting access to White Rose research papers



Universities of Leeds, Sheffield and York
<http://eprints.whiterose.ac.uk/>

This is an author produced version of a paper published in **Wear**.

White Rose Research Online URL for this paper:

<http://eprints.whiterose.ac.uk/10593>

Published paper

Tassini, N., Quost, X., Lewis, R., Dwyer-Joyce, R., Ariaudo, C., Kuka, N. (2010)
*A numerical model of twin disc test arrangement for the evaluation of railway
wheel wear prediction methods*, *Wear*, 268 (5-6), pp. 660-667

<http://dx.doi.org/10.1016/j.wear.2009.11.003>

A NUMERICAL MODEL OF TWIN DISC TEST ARRANGEMENT FOR THE EVALUATION OF RAILWAY WHEEL WEAR PREDICTION METHODS

N. Tassini ^a, X. Quost ^a, R. Lewis ^a, R. Dwyer-Joyce ^a, C. Ariaudo ^b, N. Kuka ^b

^a Department of Mechanical Engineering, University of Sheffield, Sheffield, S1 3JD, United Kingdom

^b Running Dynamics, ALSTOM Ferroviaria s.p.a., Via O.Moreno 23, Savigliano (CN), 12038, Italy

Twin disc tests are commonly used to study wear in railway materials. In this work the implementation of a numerical model of the twin disc arrangement is given, which reproduces the distribution of tangential forces over the contact patch between the two discs. Wear is subsequently calculated by relating the forces and creepage between the two discs using three different wear functions found in the literature. The resulting wear rates are compared with experimental data for discs made of common railway wheel and rail steels. This allows a comparison and assessment of the validity of the different wear algorithms considered.

Keywords: Railway wheel wear; Contact model; Wear coefficients; Twin disc testing

1. INTRODUCTION

Wheel wear prediction is a current key-topic in the field of railway research, as it has a major impact on economical and safety aspects in the design of trains. In the open literature several methods for estimating wear of railway wheels can be found. These methods are based on real wear data acquired using different experimental techniques, with the twin disc arrangement being the most common

one. This work aims at comparing three wear functions found in the literature, which were respectively developed by British Rail Research (BRR) [1], the Royal Institute of Technology from Stockholm (KTH) [2], and the University of Sheffield (USFD) [3]. The comparison is made by means of a purposely-built numerical model of a twin disc test set-up. The wear rate is obtained by relating the forces and creepage between the two discs using the three different functions. Two different approaches can be implemented: global, based on the mean values of the contact parameters, and local, by analysing the variation of the contact parameters across the discs' contact area. The resulting wear rates are compared with experimental data for discs made of common railway wheel and rail steels [3]. The aim is to compare the different methods and their implementations. Of interest is also the evaluation of the error connected with applying wear methods obtained globally in local models.

2. TWIN DISC TEST APPROACH

The twin disc test machine is designed to simulate two steel surfaces in rolling-sliding contact. The twin disc test consists of two independently driven discs held in contact with a constant applied load. The inputs are the applied normal contact load and the slip between the two discs (creep), while the outputs are the resulting tangential force and the quantity of wear. Wear is subsequently related to the contact parameters in different ways: the wear is usually expressed as wear rate (i.e. wear per cycle or distance rolled) and related to contact pressure and slip between contacting surfaces in some form. In this work an energy approach used by BRR and USFD was adopted. This makes the assumption that the material lost is proportional to the energy dissipated in the contact zone. KTH method does not compute contact energy, but was adapted to allow the comparison. Wear is expressed as mass loss in μg / distance rolled in m / contact area in mm^2 , against

the wear index $W.I.$, function of the tangential or traction force T and the slip velocity \dot{s} between the two discs surfaces. The method for its calculation is different for global and local approaches, and is described in the following section.

3. TWIN DISC MODEL

The twin disc test arrangement can be studied as two cylinders with parallel axes in rolling-sliding contact as shown in Figure 1.

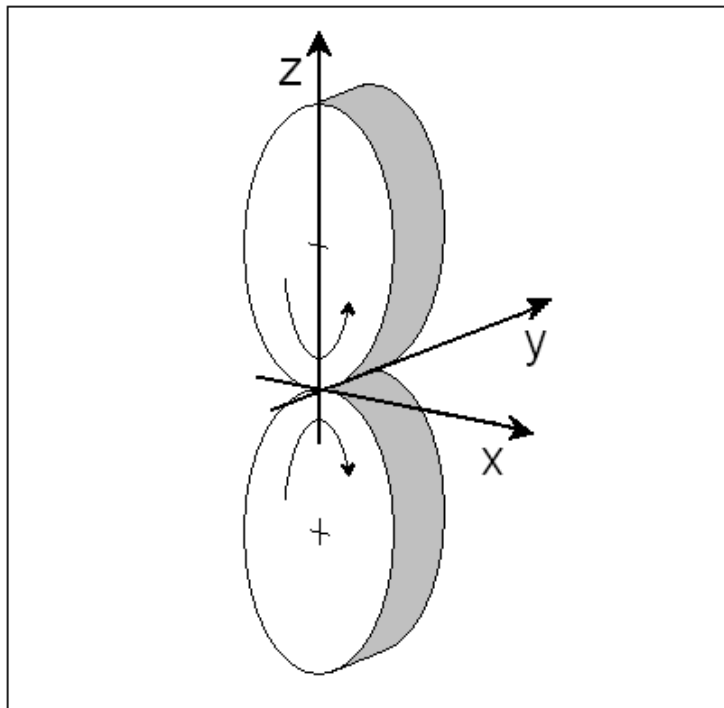


Figure 1. Twin disc arrangement diagram and reference axes system adopted.

The normal problem is solved with Hertz theory, which gives both the contact patch semi-length a and the distribution of the normal pressure at contact in the rolling direction [4]:

$$a^2 = \frac{2PR^*}{\pi E^*} \quad (1)$$

where P is the normal force, R^* is the curvature function, E^* is a measure of the compliance of the two discs, which depends on their materials' elasticities. The normal stresses are distributed elliptically along the contact patch length $2a$ with a maximum value p_0 at the centre given by

$$p_0 = \frac{2P}{\pi a}. \quad (2)$$

The sliding motion between surfaces is described by Amonton's law, which gives the value of the maximum tangential force transmitted T_f :

$$|T_f| = \mu_f P \quad (3)$$

where μ_f is the coefficient of sliding friction, whose value is related to the material properties and the physical conditions at the interface. A smaller tangential force will not give rise to complete sliding but will introduce frictional tractions which deform the bodies in shear. The interface will be divided in regions of "slip" and regions of "stick", where there will be small relative motion or adhesion respectively. The tangential problem relates to calculating the slip velocity between the contacting disc surfaces and the distribution of tangential pressure, which subsequently leads at the computation of $W.I.$. The core of a numerical model of the twin disc apparatus is thus the model of rolling-sliding contact of elastic bodies and the theory for its analytical solution is given in Ref.[4]. Of interest here is the definition of the slip velocity \dot{s} between the two discs surfaces. In the twin disc case the problem is reduced to the rolling direction, i.e. the direction of relative movement between the two discs, which lies on the plane tangent to the two disc surfaces at their contact, perpendicular to the discs' axle direction. This direction is noted in this work with x and is shown in Figure 1. As a consequence velocities along other directions and spin effects are not considered. In case of pure rolling between discs, material particles of each surface would flow through the contact region with a common velocity V known as rolling speed, directed along x , with

magnitude corresponding to the mean of the surface speeds of the two discs. In case a tangential force is transmitted at the discs' interface, a slip between discs' surfaces will arise. This slip velocity \dot{s} is given by the difference of the surface velocities v_{x1} and v_{x2} of the two discs, where the subscripts "x" stand for components along the rolling direction; the slip velocity is made of two components [4]:

$$\dot{s}_x(x) = v_{x1} - v_{x2} = v_x V + \frac{\partial u_x}{\partial x} V \quad (4)$$

where $v_x V$ is the rigid slip, i.e. the relative velocity of the two discs in case they were perfectly rigid bodies; v_x is the local creepage, that is the local percentage difference of surface speeds. The second term of the slip velocity given in Equation (4) is related to the deformations u_{x1} and u_{x2} of the two discs and the term $\partial u_x / \partial x$ arise from the state of strain in the surface, which depend on the surface tractions. Equation (4) is valid in both slip and stick regions of the contact patch, and the configuration for each region can be found from the boundary conditions [4]. The approaches for solving the twin disc rolling/sliding contact problem can be divided into two:

- global, on the whole contact patch considering the mean values of normal and tangential forces;
- local, by dividing the contact patch into small cells and evaluating the contact parameters for each cell.

3.1. Global contact model

The global computation is the most basic and most commonly used approach for describing rolling-sliding contact. The contact patch is analysed in its integrity and thus forces and creepage acting on it are considered as single values for the whole area. In the twin disc case the normal force P needed for solving the Hertz

problem (Equations (1) and (2)) is the one applied to hold together the two discs. Regarding the solution of the tangential problem and the calculation of the wear index $W.I.$, the tangential force T is obtained from the torque measured on one of the discs axes. The effect of the elastic deformation due to frictional tractions is not taken into consideration, and thus the slip velocity \dot{s} is substituted by the imposed longitudinal slip between the two discs during the tests, expressed as percentage difference in surface speeds, which is known as global creepage γ . In a global approach the wear index is calculated as a single value for the whole contact patch which corresponds to

$$W.I. = T\gamma . \quad (5)$$

3.2. Local contact model

Two different local implementations were considered during this work, one based on the “exact theory” [4], and the second based on the “simplified theory” (FASTSIM) implemented by Kalker [5]. The solutions relate to find analytical expressions for describing the deformation term of the slip $\dot{s}(x)$ in Equation (4) and the tangential stress $q(x)$ along the contact patch.

3.2.1. Exact theory

The contact patch semi-length a is found according to Equation (1): in the exact theory the adhesion region is assumed to occupy the leading edge of the contact patch and to be $2c$ long, as shown in Figure 2, where

$$c = a - \frac{V_x}{\mu_f} R^* \quad (6)$$

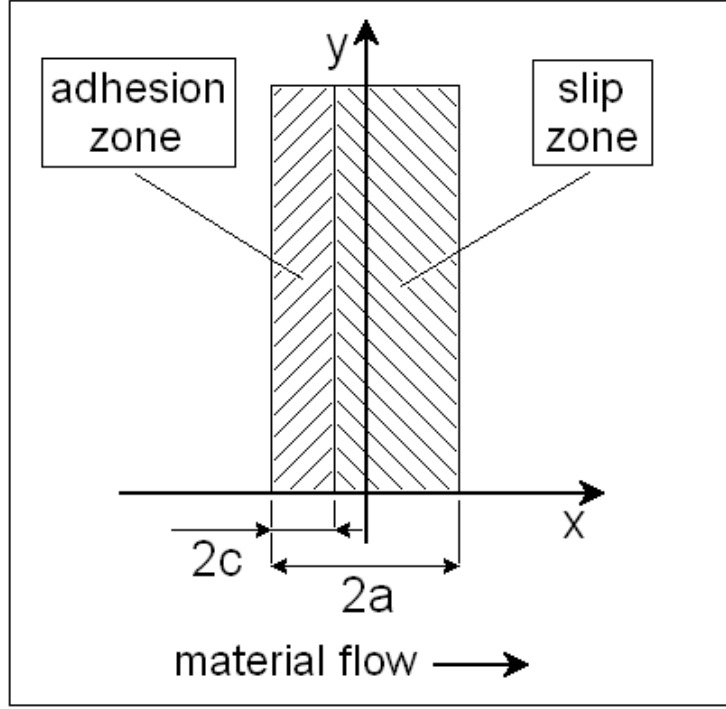


Figure 2. Geometry of discs' contact patch.

The equations for the deformation term of the slip velocities are different for the two regions of contact; assuming that the leading edge corresponds to $x = -a$:

$$\frac{\partial u_x}{\partial x} = \begin{cases} 2 \frac{\mu_f p_0}{E^*} \frac{a-c}{a} & \text{for } -a \leq x \leq -a+2c \text{ (adhesion zone)} \\ -2 \frac{\mu_f p_0}{E^*} \frac{x}{a} & \text{for } -a+2c < x \leq a \text{ (slip zone)} \end{cases} \quad (7)$$

If, according to Hertz theory, the elliptical distribution of the normal pressure is denoted with $p(x)$, also the tangential stress assumes two different forms for the two contact regions:

$$q(x) = \begin{cases} \mu_f p(x) - \frac{c}{a} \mu_f p_0 \sqrt{1 - \left(\frac{x+a+c}{c}\right)^2} & \text{for } -a \leq x \leq -a+2c \text{ (adhesion zone)} \\ \mu_f p(x) & \text{for } -a+2c < x \leq a \text{ (slip zone)} \end{cases} \quad (8)$$

3.2.2. Simplified theory

The exact theory is well-suited for one-dimensional problems, like the twin disc test. Three-dimensional problems, like railway wheel/rail contact, are instead difficult to solve with this method. Kalker developed a simplified linear theory based on an approximation of the deformation [5]

$$u(x) = L_x q(x) \quad (9)$$

where L_x is a coefficient which depends on the contact patch dimensions and on the rigidity of the materials in contact. As a consequence

$$\frac{\partial u_x}{\partial x} = L_x \frac{\partial}{\partial x} q(x) \quad (10)$$

If Equation (10) is substituted in Equation (4), $q(x)$ can be inferred in the adhesion region, where it is valid the condition $\dot{s}(x) = 0$

$$\frac{\partial}{\partial x} q(x) = \frac{v_x}{L_x} \quad (11)$$

This equation is used in an iterative algorithm for finding slip and tangential stress along the contact patch. Starting from the leading edge $x = -a$, where both slip and tangential stress are zero, the contact patch length is divided in partitions dx , and for each partition a value of tangential stress $\tilde{q}(x)$ is computed:

$$\tilde{q}(x + dx) = q(x) + \frac{v_x}{L_x} dx \quad (12)$$

The value $\tilde{q}(x + dx)$ is compared at each step with the limiting traction bound $q_{\text{lim}}(x + dx) = \mu_f p_2(x + dx)$ given by Amonton-Coulomb's law, where $p_2(x)$ is a parabolic distribution of the normal pressure; the following cases will be obtained:

$$\left\{ \begin{array}{l} \text{if } \tilde{q}(x+dx) \leq q_{\text{lim}}(x+dx) \Rightarrow \begin{array}{l} q(x+dx) = \tilde{q}(x+dx) \quad (\text{adhesion zone}) \\ \dot{s}(x+dx) = 0 \end{array} \\ \text{if } \tilde{q}(x+dx) > q_{\text{lim}}(x+dx) \Rightarrow \begin{array}{l} q(x+dx) = q_{\text{lim}}(x+dx) \\ \frac{\partial u_x}{\partial x} = L_x \frac{\partial}{\partial x} (q_{\text{lim}}(x)) \quad (\text{slip zone}) \end{array} \end{array} \right. \quad (13)$$

where the value of $\partial u_x / \partial x$ for the slip zone needs to be used in Equation (4) to obtain the slip velocity.

3.2.3. Comparison of local models

In both implementations of the local contact model, the wear index corresponds to

$$W.I. = \frac{\dot{s}(x)}{V} q(x) \quad (14)$$

computed for each partition of the contact patch, using the values obtained from equations of the previous sections.

It is possible to visualise the differences between the two local models by plotting the distribution of stresses and the slip velocities along the contact patch. Figure 3 shows normal and tangential stresses along the rolling direction. The normal stress is calculated using Hertz theory through Equation (2), and has an elliptical distribution. The tangential stress is calculated with both the exact theory and simplified theory following Equations (8) and (13), respectively. In both cases the adhesion and slip regions are visible at the left and right of the contact patch respectively. The shape of the saturated stress is elliptic for the exact theory, while is parabolic for the simplified theory, as suggested by Kalker [5]. An elliptic shape was also tried in this work with the simplified theory: using the elliptic shape for both methods, gives the exact same results for full slip conditions, while for partial slip conditions the difference is relatively small. As a consequence a parabolic distribution was adopted in this work. In Figure 4 are plotted the percentage slip velocities obtained with the two local implementations of the contact model, using

Equations (7) and (13); in the same plot is also given the value γ , which is used in the global computation of $W.I.$ in Equation (5).

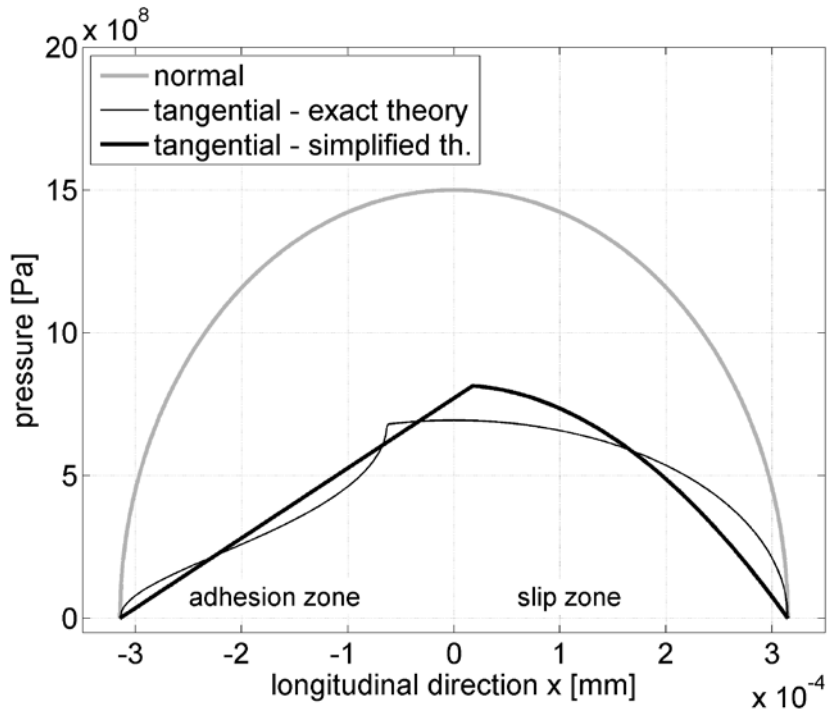


Figure 3. Distribution of stresses along contact patch.

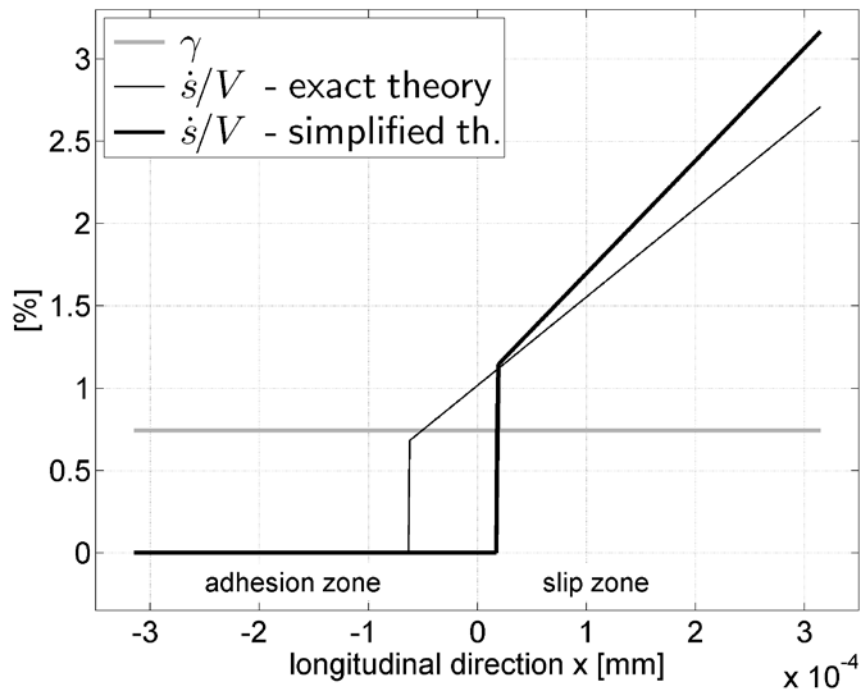


Figure 4. Slip velocities of discs' surfaces.

In the following sections, in order to compare global and local $W.I.$ values, the local $\dot{s}(x)/V$ in the slip zone of the contact patch are averaged to give a quantity corresponding to the global γ , while the tangential stresses $q(x)$ are summed to obtain a quantity corresponding to the global T . Their product gives a single $W.I.$ for the contact patch starting from the local parameters, which can be directly compared to the global $W.I.$; the two values are though not entirely comparable as the $\dot{s}(x)/V$ values refer to only the slip zone, while the global γ refer to the whole contact patch.

4. WEAR FUNCTIONS

The relation between the quantity of removed material and energy dissipated at contact is obtained from experimental data such as the twin disc. In the open literature can be found different wear functions, and here three of them were investigated:

- The British Rail Research function (BRR) [1],
- The Royal Institute of Technology function from Stockholm (KTH) [2] and
- The University of Sheffield (USFD) function [3].

4.1. British Rail Research

BRR is a global function and relates wear to the product $T\gamma$. Wear is calculated as material loss expressed in mm^2 of lost area from any radial section through the profile per km rolled, following the equations in Table 1, where D is the diameter of the wheel in mm. These equations were obtained from tests on R8T (wheel) and BS11 (rail) steels [1].

Table 1. Equations of BRR wear function [1].

T_γ [N]	Material loss [mm ²]
$T_\gamma < 100$	$\frac{0.25}{D} T_\gamma$
$100 \leq T_\gamma < 200$	$\frac{25}{D}$
$T_\gamma \geq 200$	$\frac{1.19 \cdot T_\gamma - 154}{D}$

4.2. Royal Institute of Technology – Stockholm

The KTH wear function [2] is based on Archard's wear law for calculating the volume of worn material

$$V_{\text{worn}} = k_A \frac{Pd}{H} \quad (15)$$

where P is the normal force, d is the slid distance, H is the material hardness and k_A is a coefficient dependent on normal pressure and slip velocity, given in Table 2. The values for the coefficient k_A were obtained from the analysis of three different sets of experimental data, including both twin disc and pin-on-disc results on different unspecified materials. This makes the KTH wear function material-independent. In order to obtain a wear rate directly comparable to the ones obtained with the other functions, the worn volume V_{worn} obtained with Equation (15) is then divided by the material density and the distance rolled.

Table 2. Equations of KTH wear function [2].

Pressure p [GPa]	Slip velocity \dot{s} [m/s]	k_A [-]
$p > 2.1$	any \dot{s}	$300 - 400 \cdot 10^{-4}$
$p < 2.1$	$\dot{s} \geq 0.2$	$1 - 10 \cdot 10^{-4}$
$p < 2.1$	$0.2 \leq \dot{s} < 0.7$	$30 - 40 \cdot 10^{-4}$
$p < 2.1$	$\dot{s} \geq 0.7$	$1 - 10 \cdot 10^{-4}$

4.3. The University of Sheffield

USFD algorithm is based on twin disc wear data acquired at USFD from the contact of discs made of R8T wheel material and UIC60 900A rail material [3]. These data were used to obtain the relation between wear rates and $W.I.$ values, which was expressed through the equations given in Table 3, one for each of the three wear regimes; A is the contact patch area. The parameters of these equations are the angular coefficients for mild (m_m) and catastrophic (m_c) wear regime, the wear rate value for the severe regime (q_s) and the $(W.I.) / A$ value for the transition from severe to catastrophic regime ($tr_{(s/c)}$). The $(W.I.) / A$ value for the transition from mild to severe regime is a function of the equations in Table 3 ($tr_{(m/s)} = q_s / m_m$). In the first column of Table 4 are given the values of these parameters corresponding to the twin disc test results [3].

Table 3. Equations of USFD wear function [3].

Wear regime	Wear rate
mild	$m_m \cdot \frac{W.I.}{A}$
severe	q_s
catastrophic	$m_c \cdot \frac{W.I.}{A} - (m_c \cdot (tr_{s/c}) - q_s)$

5. RESULTS

The different implementations of the twin disc model presented in the previous sections were used for analysing wear data acquired previously [3]. The purpose was to obtain the differences between the various wear functions considered in this work and their local or global implementations. The model was also used for running wear test simulations with varying input parameters, in order to study more in detail the effect of the different parameters in each wear function. The aim of

these analysis was to find the necessary corrections to be applied to each of them for obtaining the same wear predictions.

5.1. Comparison with wear data

The reference wear data analysed with the twin disc model was the dataset acquired for developing the USFD wear function described in the previous section [3]. The normal force was kept constant to give a maximum normal pressure of 1500 N/mm^2 , while the imposed slip varied in the range 0.01 - 20%. The measured tangential force data are plotted as a function of the imposed slip as the filled circles in Figure 5. The test results for high creepage values, corresponding to full slip conditions, were used to infer the friction coefficient between the wheel and rail materials studied, which was found to be 0.46. The model results are commented in the next sections.

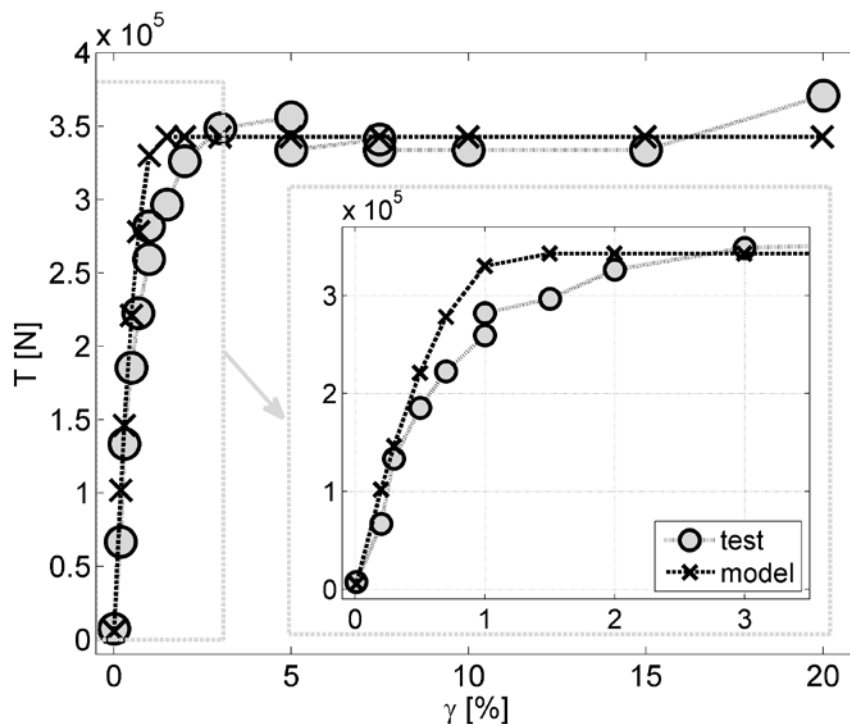
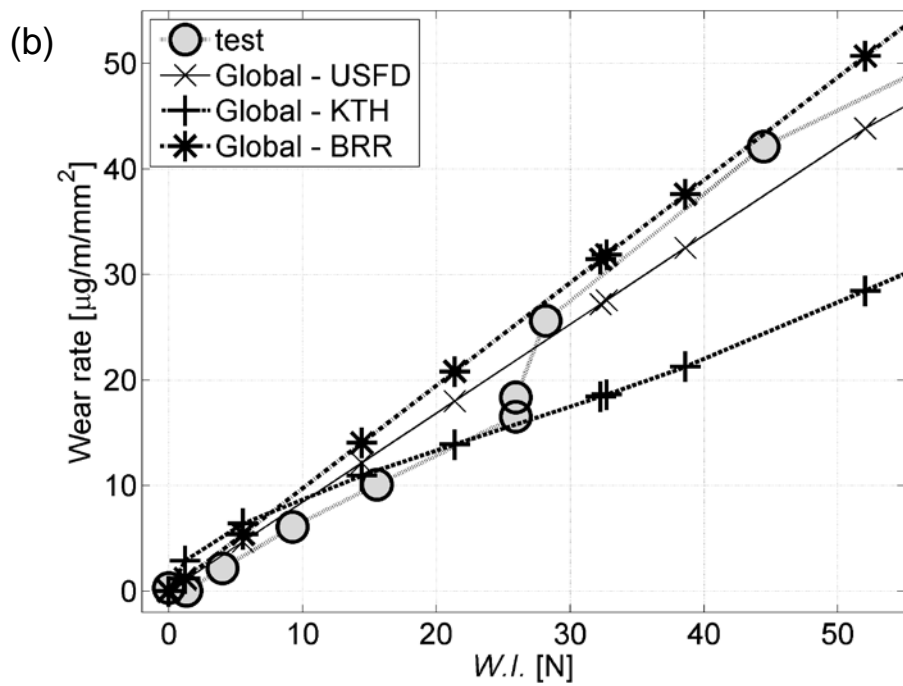
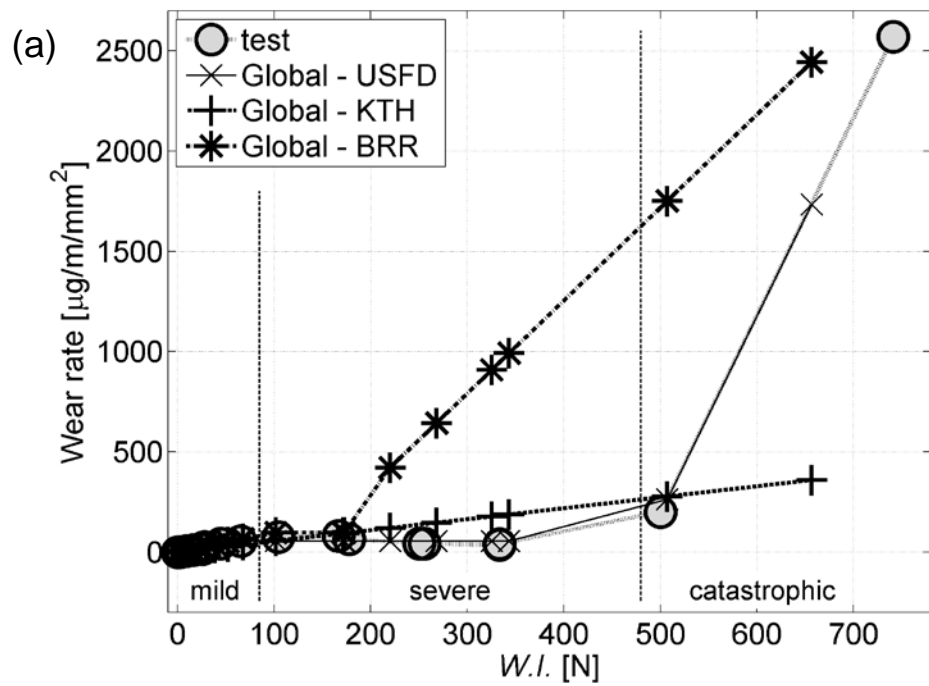


Figure 5. Tangential force from wear tests and twin disc local model.

5.1.1. Global analysis

Figure 6 shows the wear test results (filled circles) together with the wear results obtained from the three wear functions (USFD, KTH, BRR) applied globally. Wear rates are plotted as a function of $W.I.$ which in this case correspond to $T\gamma$. USFD is the wear function that better reproduces the wear experimental results, as it uses empirical coefficients of proportionality between wear and energy dissipation that were derived on this experimental dataset. Figure 6b and Figure 6c show the enlargements for the zones with $W.I.$ included between 0-70 and 50-350, which correspond to the mild and severe wear regimes respectively. Figure 6b shows that all three wear functions reproduce well the wear results in the mild wear regime. This regime roughly corresponds to tread contact conditions in real railway wheel-rail contact. Figure 6c shows that USFD wear function represents an “average” of the test results, while both KTH and BRR overestimate this type of wear. For higher $W.I.$ values, corresponding to the catastrophic wear regime, BRR wear function still overestimates wear, but seems to get closer to the test results for $W.I. > 700N$, while KTH keeps roughly the same proportionality between $W.I.$ and wear rate for all $W.I.$ values within each wear regime.



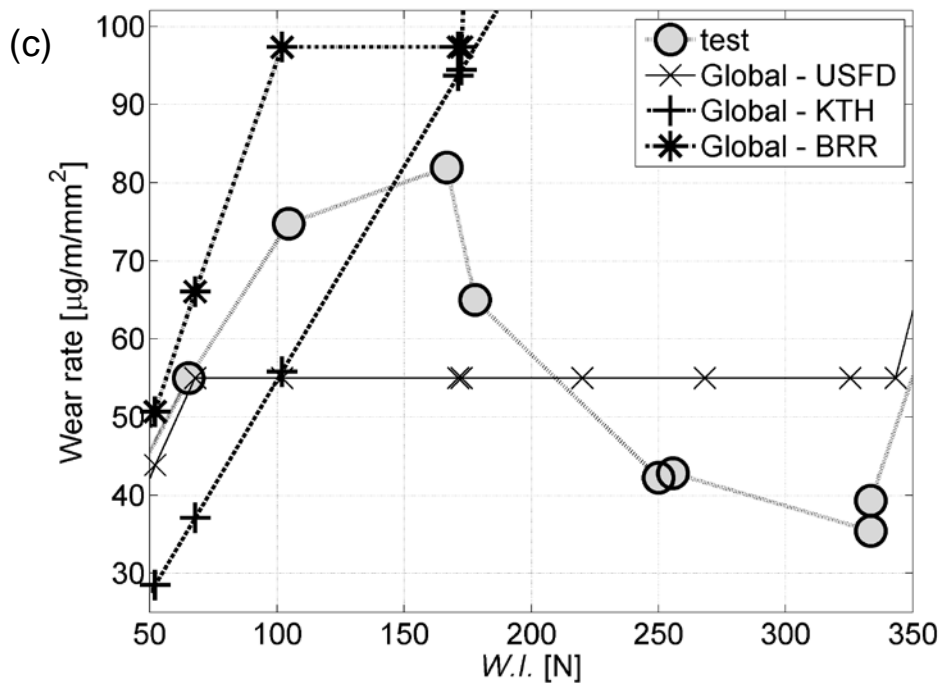


Figure 6. Global Model Results ((b) and (c) are enlargements of zones of (a)

5.1.2. Local analysis

A similar comparison was done for the local implementation of USFD and KTH wear functions compared against the twin disc results; BRR cannot be computed locally as it was originally written as a global wear function.

In Figure 5 the total tangential forces are plotted as a function of the creepage γ for the twin disc test results and for the local USFD function results, following the method described in Section 3.2.3. The two implementations following the exact and simplified theories give the same results. From the enlarged part in the dashed box, for low creepage values, the measured and simulated tangential forces differ. The model's results for high creepage values corresponding to full slip conditions appear to be an average of the test results. This is coherent with the fact that the friction coefficient value between the wheel and rail materials was obtained from

the average of these same test results. The wear rate results are plotted in Figure 7, for the tests, local USFD using the exact theory, local USFD using simplified theory, and local KTH. Both exact and simplified theories were used for computing the local KTH wear function, but they gave the same results. The results for the mild and severe regimes are very similar to the ones showed in Figure 6b and Figure 6c for the global analysis. It is clear that the KTH local wear function gives very similar results to the KTH global function, as it depends on the same parameters (i.e. normal force and slid distance). The local USFD method still gives a good approximation of wear in the mild and severe wear regime with both computations with exact and simplified theories. In the catastrophic wear regime the model overestimates wear, especially using the simplified theory.

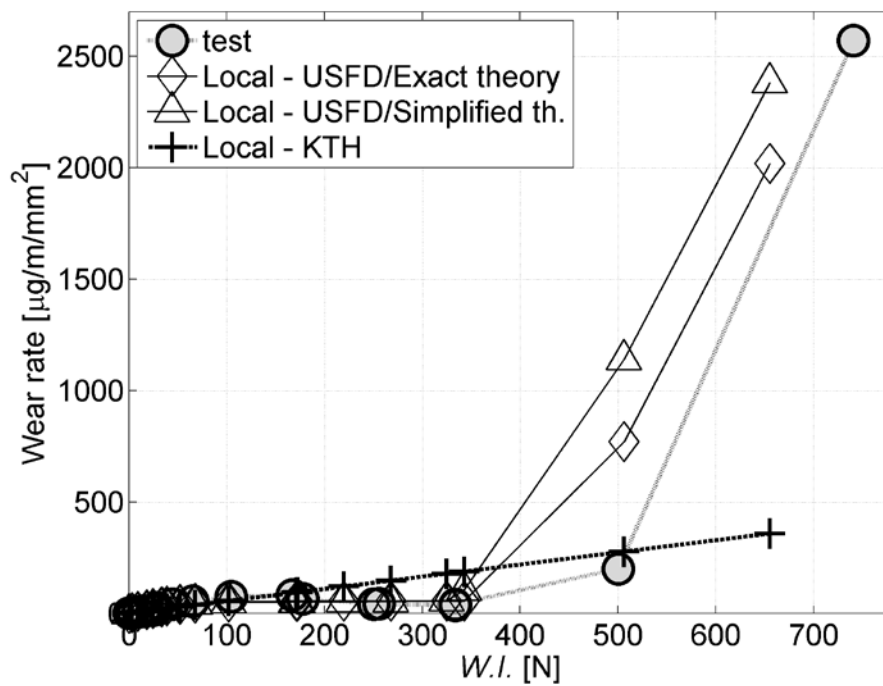


Figure 7. Local model results.

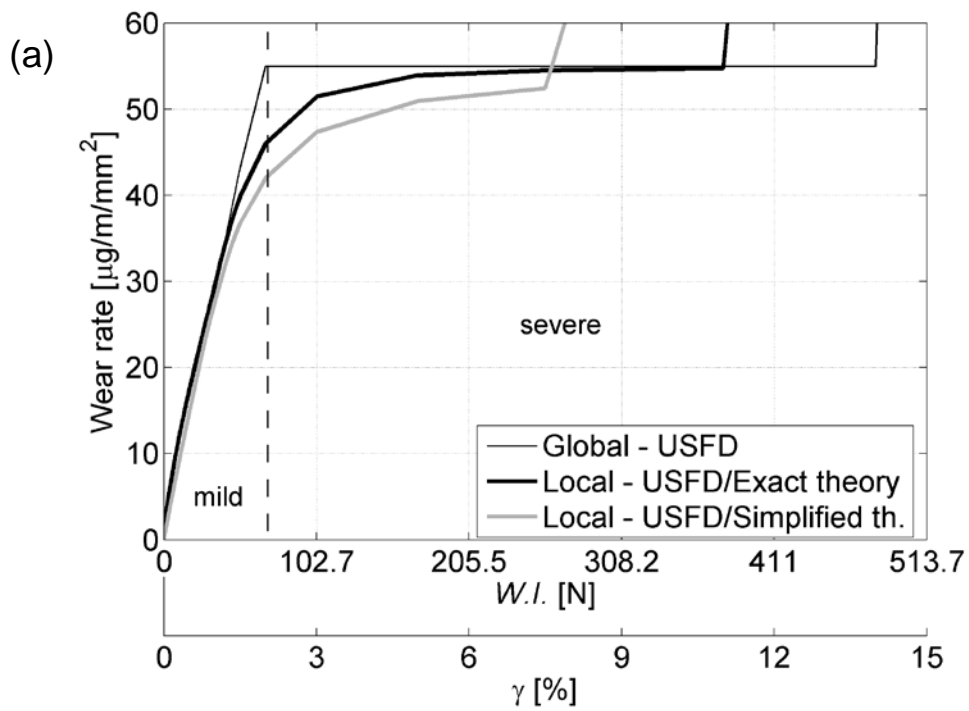
5.2. Comparison of wear functions

In order to study more in depth the differences between the different wear functions, specific wear simulations were run with the twin disc model. The simulations consist in setting two sets of calculations with varying creepage or varying normal force. Creepage was varied in the range 0.001-25% with a normal force per width of 741.43kN/m, corresponding to a maximum normal pressure of 1500 N/mm²; normal force was varied in the range 74.14-14829kN/m, with a creepage of 1%.

The first results obtained from the simulations was to show that for the KTH function the relation between wear rate and W/l is not always constant as it appears from the results of the previous sections. Following Ref.[2], changes of wear rate against contact parameters occur for surface slip velocity values of 0.2m/s and 0.7m/s and for a normal pressure value of 2.1GPa. From the simulations with varying creepage resulted that a slip velocity of 0.2m/s corresponds to a creepage above 20%, while the threshold of 0.7m/s lies out of the creepage range simulated. From the simulations with varying normal force, the threshold of 2.1GPa corresponds to a normal force of 2300kN/m. All these thresholds lie above the creepage and contact force ranges measured in the tests described in the previous section, and thus their effect could not be observed in the corresponding results.

The second purpose of the simulations was to obtain a more detailed view of the differences between global and local implementations of the USFD wear function. The results are shown in Figure 8a and Figure 8b for the mild and severe regimes and for the catastrophic wear regime, respectively. In these plots can be clearly observed the gap between the different implementations of the USFD wear function, particularly for high W/l values in the catastrophic wear regime. These results were used to find the modifications to be applied to the USFD local wear function to obtain the same results of the global implementation, which is the

closest to the twin disc results. This was achieved by modifying the parameters of the equations in Table 3; the modified parameters for obtaining wear results closer to the experimental ones with USFD local model computed with exact and simplified theories are given in the second and third columns of Table 4 respectively. These corrections allow to obtain overlapping plots for the results of Figure 8.



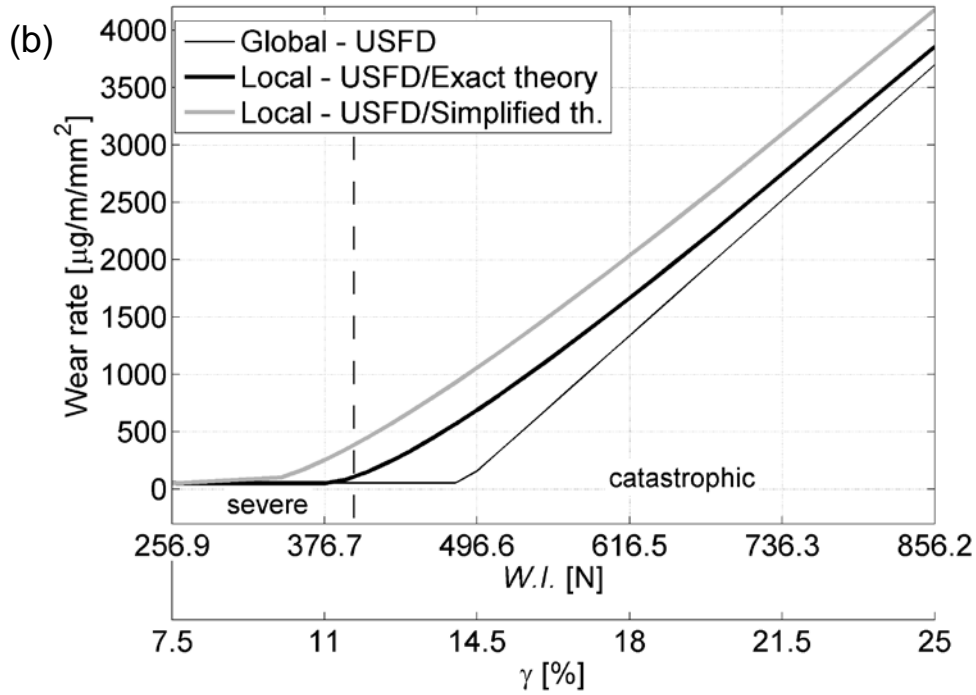


Figure 8. Wear simulations with varying creepage obtained with USFD function.

((a) mild to severe and (b) severe to catastrophic)

Table 4. Original and corrected parameters for USFD function.

	Original [3]	USFD/Exact th.	USFD/Simplified th.
m_m	5.3	5.3	5.3
q_s	55	55	56.5
m_c	61.9	83.7	83.7
$tr_{s/c}$	77.26	95	107

6. DISCUSSION

A first observation can be made on the way the wear results are plotted when they are compared with the twin disc data. As in the datasets studied the normal force P is always kept constant, the values of wear measured and simulated can be considered by function of creepage only. In Figure 9, the global USFD results of

Figure 6 are plotted with the wear results, as a function of creepage only. It is clear that the measured and simulated results do not overlap anymore, particularly at high slip levels. They overlap when plotted against $W.I.$ as the USFD wear function was built using $W.I.$ as variable – this decision was made, following also the research path of BRR, as the results were intended to be used in railway applications, where $W.I.$ is an important parameter. To explain why the wear results against creepage do not overlap, it must be taken into consideration the wear estimation procedure adopted in this work, made of two steps: the contact model, which from slip between surfaces and normal contact force, gives the corresponding $W.I.$, and the wear function which relates this $W.I.$ to the quantity of wear. As in this case the wear function is for all datasets the same (USFD), the difference must come from the contact model. The twin disc test apparatus can be considered as a contact model, whose input is a prescribed slip and a normal contact force, and outputs a $W.I.$ value between the two discs. In order to build the USFD wear function, the $W.I.$ was calculated by using the output tangential force between the two discs and the slip imposed to them. As a prescribed slip between two discs is very difficult to obtain and maintain, the difference between the results of Figure 6 and Figure 9 can be simply due to the fact that the prescribed slip value used for building the USFD wear function does not correspond to the real slip between discs. In any case the levels of error that this might involve, are well within the levels of error naturally involved during wear measurements.

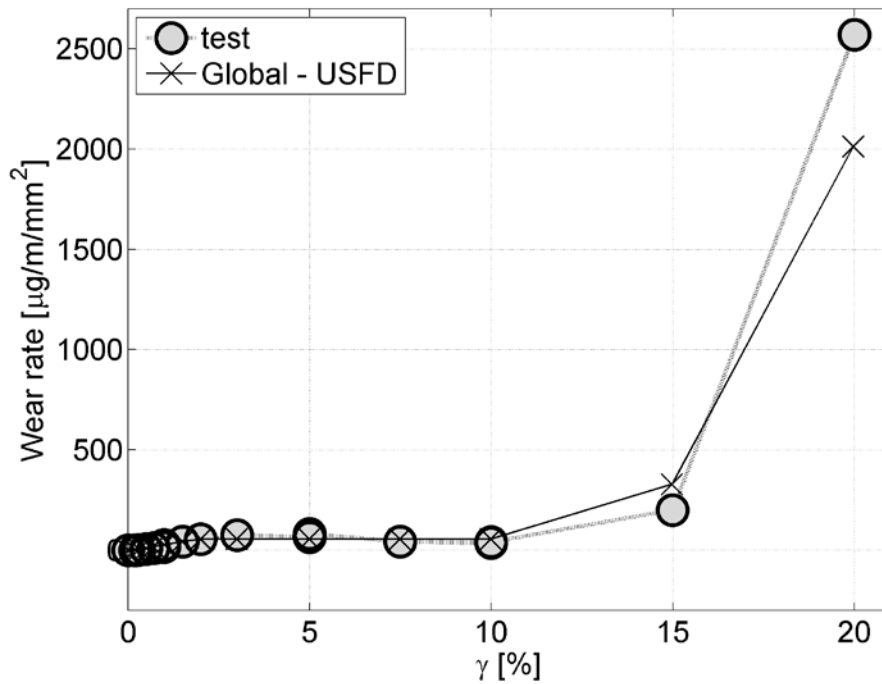


Figure 9. USFD global model results as a function of creepage.

The first purpose of this study was to compare the different wear functions. The differences can be clearly observed from Figure 6 and are related to the original experimental data used to build each of the different wear functions. In this work the reference wear function is the USFD one. The data used for its implementation was described in the previous section. The BRR wear function is also based on twin disc results. These two wear functions are very similar, the main difference being basically the shorter *W.I.* range of validity of the severe wear regime of BRR, which accounts for the higher wear rates at high *W.I.* values. This aspect could be related to the different rail materials tested. The KTH wear function appears to be sensibly different from the USFD function. This can be related to the different materials tested for their implementations and also to the different contact parameters used for characterising wear, i.e. slip velocity and normal contact pressure for KTH, and creepage and tangential pressure for USFD. A further difference between these two wear functions relates to the different relations

between contact parameters and quantity of wear. This is clear when plotting the wear simulation results for USFD and KTH wear functions as a function of creepage only, as shown in Figure 10. If this plot is compared with the results of Figure 6b, KTH function appears to be linear in respect of creepage, differently from USFD. This is related to the fact that in the USFD wear function the tangential force is constant when full slip conditions apply, but depends on creepage through the traction coefficient, when partial slip conditions exist, thus making wear a function of the square of creepage. The creepage range shown in Figure 10 corresponds to the partial slip conditions. For higher creepage values, corresponding to full slip conditions, both wear functions appear to be linear. BRR wear function poses a similar behaviour to the USFD function, as they are based on similar relations.

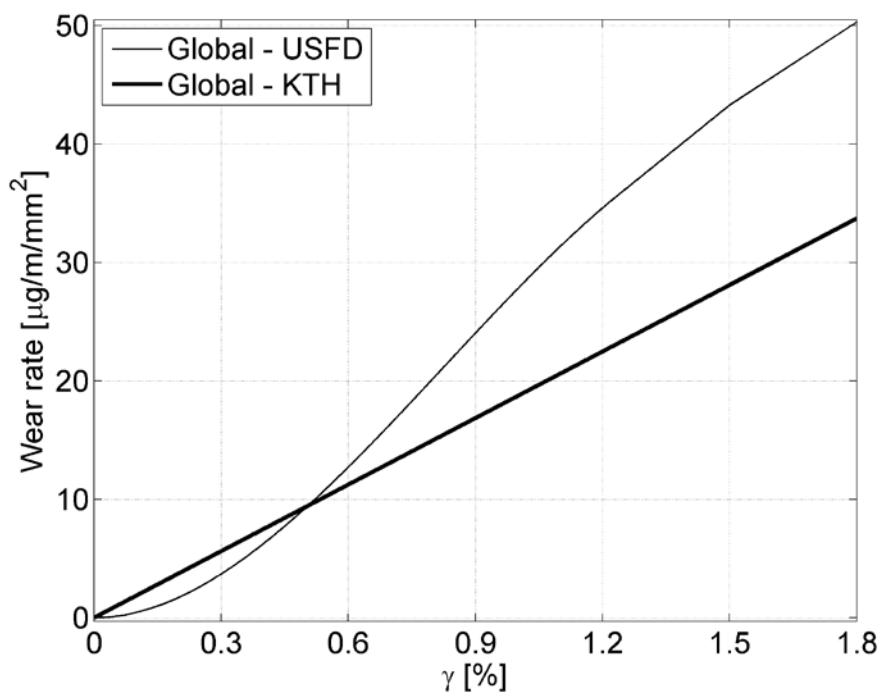


Figure 10. USFD and KTH wear results as a function of creepage.

The second purpose of this work was to study the difference between global and local implementations of the wear functions. As it was not possible to implement a

local version of the BRR function, and as the global and local versions of the KTH function basically give the same results, these considerations can be done for the USFD function only. As shown in the previous section, the main difference relates to the wear results in the catastrophic regime. It was also shown that it is possible to find the corrective parameters, provided that the original twin disc data are available. These results show that during the selection of a wear function for a given analysis, it is important to consider the nature of the problem to be solved and of the model used for its solution. Railway wheel wear analysis can be solved by taking either global or local approaches, depending on the problem's conditions and resources available. In this work it was shown that wear functions can in most cases be applied both locally or globally. In case they are applied differently from how they were originally compiled, their parameters should be checked against real data, and corrected if necessary. Of course this was for the 2D case. For 3D other considerations exist such as spin and lateral creepage, but explained below the wear approaches have been used in 3D modelling of a full scale wheel/rail contact.

The work presented, leads to the implementation of additional research:

- run new twin disc analysis on different types of railway materials, to study the effects on the USFD wear function;
- apply the different wear functions to railway wheel wear prediction models, to compare their results with field-data, in order to verify their validity.

It should be noted that the USFD wear modelling approach has in fact already been combined with multi-body dynamics simulations to predict wheel profile evolution on a full-scale roller rig [6]. The results compared well indicating the applicability of the wear testing and modelling approach to full-scale applications. $T\gamma$ values and associated wear rates from twin disc tests and full-scale tests have previously been compared and found to be similar in value [3, 7]

7. CONCLUSIONS

In this work a numerical model of a twin disc apparatus has been presented. Twin disc tests are used to characterise the wear of railway wheel and rail materials.

The relation between wear and contact parameters was studied in depth and the main points discussed are:

- wear functions are based on rolling/sliding contact models, which can be global or local, depending on the approach adopted for their implementation;
- if a wear function is applied with the other approach than the one used for its development, its parameters need to be checked against real data;
- different wear functions can be found in the literature, which give differing results, mainly due to the different nature of the datasets they are built on;
- wear simulations allowed to find the corrective parameters for using the USFD wear function, originally developed using a global approach, in local problems.

8. ACKNOWLEDGMENTS

This research project has been supported by a Marie Curie Transfer of Knowledge Fellowship of the European Community Sixth Framework Programme under contract number MTKI-CT-2006-042358. The authors also acknowledge the active support provided by the host institution ALSTOM Transport during this research.

9. REFERENCES

- [1]. T.G. Pearce, N.D. Sherratt, Prediction of wheel profile wear, *Wear* 144 (1991) 343–351
- [2]. T. Jendel, Prediction of wheel profile wear – comparisons with field measurements, *Wear* 253 (2002) 89–99

- [3]. R. Lewis, R. Dwyer-Joyce, Wear mechanisms and transitions in railway wheel steels, Proc. ImechE. part J: J. Engineering Tribology 218 (2004) 467– 478
- [4]. K.L. Johnson, Contact Mechanics, Cambridge University Press, Cambridge, 1985.
- [5]. J.J. Kalker, A fast algorithm for the simplified theory of rolling contact, Vehicle System Dynamics 11 (1982) 1-13
- [6]. F. Braghin, R. Lewis, R.S. Dwyer-Joyce, S. Bruni, A mathematical model to predict railway wheel profile evolution due to wear”, Wear, 261 (2006) 1253-1264.
- [7]. R. Lewis, U. Olofsson, Mapping rail wear regimes and transitions Wear, 257 (2004) 721-729.

FIGURES CAPTIONS

Figure 1. Twin disc arrangement diagram and reference axes system adopted.

Figure 2. Geometry of discs' contact patch.

Figure 3. Distribution of stresses along contact patch.

Figure 4. Slip velocities of discs' surfaces.

Figure 5. Tangential force from wear tests and twin disc local model.

Figure 6. Global model results.

Figure 7. Local model results.

Figure 8. Wear simulations with varying creepage obtained with USFD function.

Figure 9. USFD global model results as a function of creepage.

Figure 10. USFD and KTH wear results as a function of creepage.

APPENDIX 1. LIST OF NOTATIONS

BRR British Rail Research

KTH Royal Institute of Technology of Stockholm

USFD University of Sheffield

A area of contact patch

E^* measure of compliance of two discs

L Kalker coefficient for simplified theory

P normal contact force

R^* is the curvature function,

T tangential force

T_f maximum tangential force transmitted

V rolling velocity

$W.I.$ wear index

a contact patch semi-length along rolling direction

c adhesion region semi-length along rolling direction

m_c angular coefficients for catastrophic wear regime in USFD wear function

m_m angular coefficients for mild wear regime in USFD wear function

p normal pressure

p_0 maximum normal pressure at contact

q tangential traction

\tilde{q} iterative tangential traction in simplified theory

q_{lim} limiting tangential traction in simplified theory

q_s wear rate value for severe regime in USFD wear function

\dot{s} slip velocity

$tr_{(m/s)}$ (W.I.) / A value for the transition from mild to severe regime in USFD wear function

$tr_{(s/c)}$ (W.I.) / A value for the transition from severe to catastrophic regime in USFD wear function

u surface deformation

v surface velocity

x rolling direction

γ global creepage (percentage difference in surface speeds)

μ_f friction coefficient

ν local creepage